http://www.sciencedirect.com/science/article/pii/S0169131713001944

DOI: 10.1016/j.clay.2013.06.024

(http://dx.doi.org/10.1016/j.clay.2013.06.024)

CHARACTERISATION OF POSSIBLE PHOENICIAN POTTERY PRODUCTION OF TYRE

E. Miguel Gascón, J. Buxeda i Garrigós

Applied Clay Science, 82, 79–85 (2013)

Highlights

- The probable Tyrian products were characterized.
- The variability exhibited points to the use of a non standardized recipe.
- Production technology is based on low fired high calcareous pastes.
- Possible secondary baryte has been observed in all examined specimens.
- Ceramics of other origins were also identified.

CHARACTERIZATION OF POSSIBLE PHOENICIAN POTTERY PRODUCTION OF TYRE

Eva MIGUEL GASCÓN[1], Jaume BUXEDA i GARRIGÓS[2]

1- Instituto de Lenguas y Culturas del Mediterráneo y Oriente Próximo (ILC), Centro de Ciencias Humanas y Sociales (CCHS), Consejo Superior de Investigaciones Científicas (CSIC), C/Albasanz 26-28, 28037 Madrid (Spain) (eva.miguel.gascon@cchs.csic.es).

2- Cultura Material i Arqueometria UB (ARQ|UB, GRACPE), Dept. de Prehistòria, Història Antiga i Arqueologia, Facultat de Geografia i Història, Universitat de Barcelona, C/ de Montalegre, 6, 08001 Barcelona (Catalonia, Spain) (jbuxeda@ub.edu).

Abstract

Very few archaeometric studies have been conducted on the Iron Age sites of Lebanon. Indeed, there is a great imbalance in the information published on fabric analysis in the Levant. Most of the bibliography comes from sites located in Palestine and therefore in recent years the characterization of metropolitan Phoenician pastes is based up on proxy data. In an attempt to provide direct information about the characteristics of Phoenician production, 101 fragments of pottery from the necropolis of Tyre – Al Bass have been sampled. All individuals have been analyzed by means of X-ray fluorescence (XRF) and X-ray diffraction (XRD) analyses in order to shed light on chemical and mineralogical information to define reference groups and the technology employed in production. Furthermore, selected samples, according to the previous results, have been

further analyzed by means of scanning electron microscopy (SEM) in order to shed light on microstructure and vitrification stage. Thus, the present study represents the first steps towards the characterization of the Phoenician ceramics of Tyre in order to describe different fabrics and to differentiate possible production groups.

Introduction

Since 1997 a multidisciplinary team led by Prof. María Eugenia Aubet (Universitat Pompeu Fabra, Barcelona) has been working on the Phoenician cemetery of Tyre - Al Bass in Lebanon dated to Iron Age II (ca. 850-550 BC). The site was located on an ancient beach of lacustrine environment that is nowadays ca. 500 m away from the seashore (Aubet, 2004). Along these lines, we should note that an environmental study carried out during the 1997 and 1999 archaeological missions (Carmona and Ruiz, 2004) enabled reconstruction of the paleolandscape of the Al Bass area. These authors concluded that in the past, this area was a lagoon. In fact, there exist some old maps showing that this terrain was swamped at least until 1864. Thus, fluvial deposits would have filled the ancient lagoon through the last centuries, and ceramics seem to be buried in sandy strata, affected nowadays by strong fluctuations of groundwater level.

In 2011, 101 pots, jugs, plates, and urns, of coarse ware, red slip ware, and concentric circles decoration were sampled (Table 1). Restrictions given by the archaeological mission forced us to sample material from the general context of the paleobeach where the cemetery is located, thus any of these ceramics can be related to a specific tomb. All individuals were archaeologically classified as belonging to the Tyrian local production according to their macroscopic characteristics by naked eye. Thus, the main objective of this study was the chemical and technological characterization of the Tyrian production.

Eva Miguel Gascón 26/2/13 17:50
Comentario: Table 1

Methods

To characterize the chemical composition of all 101 samples, X-ray fluorescence (XRF) was applied. First, all superficial layers of the potsherds were mechanically removed, samples were powdered and homogenized in a tungsten carbide mill, and dried in an oven overnight. Major and minor elements were determined by preparing duplicates of glass beads (dilution 1:20) of 0.3 g of specimen mixed up with 5.7 g of lithium tetraborate ($Li_2B_4O_7$), melted in a fully-automatic bead preparation system PANalytical Perl'X-3 at a temperature of 1125 ºC. Trace elements were determined by powdered pills made from 5 g of the powdered specimen mixed up with 2 ml of a solution of n-butylmethacrylate synthetic resin (Elvacite 2044, in 20 % acetone). The quantification of the concentrations was performed using an Axios^{mAX}-Advanced PANalytical spectrometer with an Rh excitation source using a calibration line performed with 56 International Geological Standards. Interferences were taken into consideration and matrix effects were corrected by using the PANanalytical Pro-Trace software for trace elements. The elements determined comprised Fe_2O_3 (as total Fe), Al_2O_3, MnO, P_2O_5, TiO_2, MgO, CaO, Na_2O, K_2O, SiO_2, Ba, Rb, Mo, Th, Nb, Pb, Zr, Y, Sr, Sn, Ce, Co, Ga, V, Zn, W, Cu, Ni and Cr. Loss of ignition (LOI) was determined by firing 0.3 g of dried specimen at 950 ºC during 3 h.

The mineralogical composition was studied by means of X-ray diffraction (XRD). Measurements were made using a Bragg-Brentano geometry PANalytical X'Pert PRO MPD Alpha-l diffractometer (radium = 240 mm) working with the Cu-Kα radiation (λ = 1.5406 Å) (45 kV – 40 mA) equipped with an X'celerator detector. Measurements where taken from (4 to 100)º2Θ with a measure step of 0.017º2Θ and an acquisition time of 50 s per step. Evaluations of the crystalline phases present in each analyzed

individual have been evaluated with the software package DIFFAC/AT Siemens that includes the database of the *International Centre for Diffraction Data, Joint Committee of Powder Diffraction Standards*, 2006 (ICDD-JCPDS).

Finally, some specimens in representation of the different chemical groups and their fabrics as well as those that showed some peculiarities in their chemical data (TAB003, TAB005, TAB007, TAB012, TAB014, TAB017, TAB022, TAB042, TAB054, TAB070, and TAB100) were selected for analysis with scanning electron microscopy (SEM) attached to an energy-dispersive X-ray analyser (EDX) in order to characterize the microstructure, the sintering stage of the ceramic's matrix and to identify aplastic inclusions. Thus, fresh fractures of the observed samples were coated with a carbon layer in a high vacuum atmosphere. An acceleration voltage of 20 kV, beam current of 1 nA, and 100 s per microanalysis was used.

Chemical Results

The elemental concentrations determined by means of XRF are a special case of the projective d+1-dimensional space, the simplex S^d. Projective points are represented by a d+1-dimensional vector of coordinates adding up to a constant k ($k \in R^+$),

$$\mathbf{x} = [x_1,..., x_{d+1}] \mid x_i \geq 0 \ (i = 1,..., d + 1), \ x_1 + \ldots + x_{d+1} = k,$$

(in the present case, k = 100), a subset in the positive orthant R_+^{d+1}, following a multiplicative model with a logarithmic interval metrics (Barceló-Vidal *et al*. 2001, Aitchison 2005, Buxeda 2008). Therefore, for the statistical data treatment, raw concentrations have been ALR transformed, according to

$$\mathbf{x} \in S^{\mathbf{d}} \rightarrow \mathbf{y} = \log\left(\frac{\mathbf{x}_{-\mathbf{D}}}{\mathbf{x}_{\mathbf{D}}}\right) \in R^{\mathbf{d}}$$

being S^d the d-dimensional simplex, $\mathbf{x}_{-D} = [x_1,...,x_d]$, and D = d + 1, or CLR transformed, according to

$$\mathbf{x} \in S^{\mathbf{d}} \rightarrow \mathbf{z} = \log\left(\frac{\mathbf{x}}{\mathbf{g}(\mathbf{x})}\right) \in R^{\mathbf{D}}$$

being S^d the d-dimensional simplex, and g(**x**) the geometric mean of all D (D = d + 1) components of **x** (Aitchison 1986, Buxeda 1999). Moreover, several elements were discarded: Mo and Sn due to analytical imprecision, and Co and W because of the possible contaminations from the tungsten carbide cell of the mill.

The compositional variation matrix enabled the quantification of the total variation (*vt*) present in the data matrix and the investigation of the source of this variability. In this case, the *vt* should be considered high (*vt* = 2.69318). This value suggests these data have a polygenic character, which means that not all individuals exhibited similar compositions; so, following the provenance postulate, it would be expected that they represent different units of production (Buxeda and Kilikoglou 2003). The evenness chemical variability graph (Figure 1) shows that most of the chemical variability is linked to Pb, Cr and, especially, MnO, Ba and Na_2O. Contrariwise, it is also clear that TiO_2 is the element that imposes the lowest relative variation when used as divisor in ALR transformation and will (Buxeda 1999), therefore, be used in the statistical data treatment. Because of the extreme variability introduced by Na_2O, Ba and MnO these

Jaume Buxeda i Garrigós 13/4/12 15:32
Comentario: Figure 1

elements were not included in the statistical data treatment. Also, Pb, Cu and P_2O_5 were not used because they are known to be sensitive to post-depositional perturbations.

A first cluster analysis was performed with S-Plus 2000 (MathSoft 1999) software, using the square Euclidian distance and the centroid agglomerative algorithm on the subcomposition Fe_2O_3, Al_2O_3, MgO, CaO, K_2O, SiO_2, Rb, Th, Nb, Zr, Y, Sr, Ce, Ga, V, Zn, Ni and Cr, ALR transformed using TiO_2 as divisor. Globally, it can be said that all individuals exhibit high levels of CaO (between 19.58% and 43.11% in normalised data). However, the study of the dendrogram (Figure 2) shows that, while 89 out of 101 individuals can be identified as forming a large group (labelled AB), still 12 individuals are clear outliers (TAB011, TAB012, TAB016, TAB017, TAB024, TAB031, TAB038, TAB039, TAB051, TAB067, TAB079, TAB093), having very different chemical compositions in relation to group AB, but also among themselves (Table 3).

Jaume Buxeda i Garrigós 26/2/13 17:52
Comentario: Figure 2

Further examination of the 89 individuals included in group AB was done by performing a second cluster analysis on the same subcomposition as before but excluding the 12 outliers. Now, a structure in three different subgroups accounting for 71 out of 89 samples (mainly AB1 to AB3) can be seen in the dendrogram (Figure 3), while the 18 samples left are not place in these subgroups. The main differences between AB1 and AB2 are clearly related to the CaO and Sr relative contents, higher in AB1 (Table 2). These higher concentrations seem to be related to a coarser nature of pastes in subgroup AB1, and do not have any archaeological counterpart. Indeed, in both subgroups, plates and jugs are mixed, as well as the different surface treatments recorded (plain, painted and red slip).

Jaume Buxeda i Garrigós 26/2/13 17:52
Comentario: Figure 3, Table 2, Table 3

The repetition of the data cluster analysis, not considering CaO and Sr, leads to the fusion of subgroups AB1 and AB2. Regarding subgroup AB3, its lower Ni content seems to suggest a separate group. Nevertheless, an iterative calculation of Mahalanobis distances to AB1 centroid, even considering CaO and Sr, leads to a unique group (AB) including all 89 individuals. These results clearly point to a single group, with a relatively high variability, even if some structure can be observed within it.

Regarding the 12 outliers, no conclusions can be drawn to present. However, it must be noticed that TAB012, which exhibits very high Cr and Ni contents (6359 ppm and 1504 ppm respectively, in normalized data, see Table 3), shows a very different chemical composition. Considering the historical commerce contacts between Tyre and Cyprus, the provenance of this jug can be tentatively related to somewhere in this island. In fact, the archaeological study focus on the typology and chronology of the necropolis ceramics, has already detected the use of Cypriot pottery as urns or even among the pottery objects that accompany them (Aubet and Núñez, 2008). The high MgO and CaO content in specimen TAB017 (11.63 % and 42.91 % respectively, in normalized data, see Table 3), related to the probable presence of abundant dolomite should also be noted. From an archaeological point of view it is also interesting to see how individuals TAB031 and TAB067 stand as outliers (Table 3). TAB031 corresponds to the only urn fragment analyzed in this study, while TAB067 is a neck-ridge jug with a painted decoration of concentric circles, stylistic fact that makes us considered it the oldest sample analyzed (Bikai 1978, Núñez 2004).

Finally, a more surprising result is related to the very high (even extreme) Ba content in all individuals. Along these lines, it must be highlighted that the highest content is

exhibited by individual TAB042 (31518 ppm, on normalized data). Such high numbers, however, are related to determinations of Ba concentrations over 2000 ppm, which is the upper regression limit and must be, therefore, considered as semiquantitative under the present analytical conditions (Figure 4).

Jaume Buxeda i Garrigós 13/4/12 18:36
Comentario: Figure 4

Mineralogical and microstructural results

The chemical data indicates that the majority of the individuals can be considered as calcareous (5-6 % < CaO < 15-20 %) or even better as highly calcareous (CaO > 15-20 %) pottery. The latter type is usually fired at low temperatures in order to avoid dissociation of primary calcite that will allow the apparition of an excess of unreacted CaO after firing. This excess of CaO will then reform calcium carbonate, with a significant increase in volume that will cause pottery to crumble away after the internal multiple pressures (Picon 1973; Maniatis *et al.* 1981, 1983; Tite *et al.* 1982; Tschegg *et al.* 2009). The situation of most of the individuals of the three subgroups inside the ceramic triangle (Figure 5) is located in the thermodynamic equilibrium triangle of quartz-anorthite-wollastonite, characteristic of calcareous pottery (Heimann 1989). Some individuals of AB2 (TAB022, TAB025, TAB029, TAB035, TAB036, TAB040, TAB042, TAB047, TAB050, TAB061, TAB080, TAB090, TAB095 and TAB100), one of AB1 (TAB060) and one of AB3 (TAB052), are inside the thermodynamic equilibrium triangle wollastonite-anorthite-gehlenite, which is characteristic of highly calcareous products.

Jaume Buxeda i Garrigós 15/4/12 13:15
Comentario: Figure 5

As expected, XRD results enable the estimation of a low equivalent firing temperature (EFT) for individuals in AB group (below 800 ºC), since no firing phases are observed (Figure 6, upper left). In addition that baryte can be observed by XRD in individual

TAB042 (Figure 6, upper right), and dolomite is clearly observed in the outlier individual TAB017 (Figure 6, lower right). The latter can also be considered as low fired, since no firing phases are present and calcite and, especially, dolomite are detected (Echallier 1984). Finally, regarding the outlier individual TAB012 (Figure 6, lower left), amphibole is clearly present, reinforcing its hypothetical Cypriot provenance (Aström 1972; Bieber 1978; Atalar and Kilic 2006; Tschegg et al. 2009). In this case, estimation of EFT is problematic, due to the lack of other individuals of the same production that allow a comparison.

Jaume Buxeda i Garrigós 13/4/12 18:36
Comentario: Figure 6

Results of SEM show that individuals in the AB group exhibit a typical non-vitrified matrix (Figure 7, individual TAB003). EFT can then be estimated below 700-750 ºC. Moreover, the matrix shows the presence of abundant microfossils and calcareous inclusions, typical of those individuals. SEM examination has also enabled the observation of baryte in all examined individuals. Even if it is difficult to identify if this baryte is primary or secondary, in several cases its secondary origin is clear. In such cases, baryte is detected inside voids, in different morphologies (Figure 7, TAB070). Even if the secondary nature of these baryte crystals seems clear, its origin and mechanism still have to be studied and further work is still needed. Regarding outlier individual TAB017 rhombohedral inclusions were found, pointing to a possible addition of dolomite as temper (Figure 7, TAB017). Finally, the outlier individual TAB012 exhibits a matrix in an initial vitrification / continous vitrification (Vc-) stage. Thus, EFT can be estimated in the range 750 - 850 ºC (Figure 7, TAB012), which is higher than the usual firing temperatures estimated for individuals in group AB.

Jaume Buxeda i Garrigós 13/4/12 18:35
Comentario: Figure 7

Final remarks

Thanks to this preliminary study it has been possible to characterize by chemistry and SEM the Phoenician pottery found in the cemetery of Tyre - Al Bass. Tyrian productions were identified in the larger AB group, as well as possible Cypriot ones (TAB012), and several other productions (up to 11) represented by single sample. The absence of technological variations among the different archaeological shapes and types studied, point to the fact that similar clays and temper were used in a production technology based on the use of high calcareous pastes fired at low temperatures. Nevertheless, the variability exhibited in the chemical data also seems to point to the use of a non-standardized recipe in the paste preparation.

Secondary baryte has been observed in all examined individuals, and must be related to the high Ba concentrations determined by XRF. Its presence could be related to some extent to a weathering phenomenon, but still needs to be carefully studied.

Much more work is clearly needed, but the results achieved to date shed light on the Tyrian pottery production and its technology, but also show a complex picture of ceramics of diverse origins arriving at the site.

Acknowlegements

This study was possible thanks to Tyre - Al Bass project directed by Dr. María Eugenia Aubet and the Direction Génerale d'Antiquités du Liban for its permission to study these materials. We are also indebted to Dr. Francisco J. Núñez Calvo for archaeological information.

Eva Miguel Gascón is indebted to the JAE-Predoc programme funded by the CSIC. All the analyses presented were carried out in the Centres Científics i Tecnològics de la Universitat de Barcelona.

References

Aitchison, J., 1986. The Statistical Analysis of Compositional Data, Chapman and Hall, London.

Aitchison, J., 2005. A concise guide to compositional data analysis. 2nd Compositional Data Analysis Workshop – CoDaWork'05, http://ima.udg.edu/Activitats/CoDaWork05/A_concise_guide_to_compositional_data_analysis.pdf. Girona: Universitat de Girona.

Anderson, R. L., 1987. Practical Statistics for Analytical Chemistry, Van Nostrand-Reinhold, New York.

Aström, P., 1972. The Middle Cypriote Bronze Age: Architecture and Pottery, vol. 4. The Swedish Cyprus Expedition, Lund, p. 1C.

Atalar, C., Kilic, R., 2006. Geotechnical properties of Cyprus clays. Engineering Geology for Tomorrow's Cities, The 10th IAEG Congress, Nottingham, paper 419. Geological Society of London.

Aubet, M. E., 2004. The Phoenician Cemetery of Tyre-Al Bass. Excavations 1997-1999, Bulletin d'Archéologie et d'Architecture Libanaises I, Beirut.

Aubet, M. E., Núñez, F. J., 2008. Cypriote imports from the Phoenician cemetery of Tyre, Al-Bass. In: Doumet-Serhal, C. (Ed.), Networking patterns of the Bronze and Iron Age Levant. The Lebanon and its Mediterranean connections, Archaeology and History of Lebanon, Beirut, 71-104.

Barceló-Vidal, C., Martín-Fernández, J.A., Pawlowsky-Glahn, V., 2001. Mathematical foundations of compositional data analysis. In G. Ross (Ed.), Proceedings of IAMG'01-The annual meeting of the International Association for Mathematical Geology, 6-12 September 2001, Cancún, México, pp. 1-20. CD-ROM.

Bieber, A. M., 1978. Neutron Activation Analysis. The Pottery of Tyre, in P. M. Bikai, Pottery of Tyre, Aris & Phillips, Warminster, pp. 88-90

Bikai, P. M., 1978. Pottery of Tyre, Aris & Phillips, Warminster.

Buxeda i Garrigós, J., 1999. Alteration and Contamination of Archaeological Ceramics: The Perturbation Problem, Journal of Archaeological Sciences, 26, 295-313.

Buxeda i Garrigós, J., 2008. Revisiting the compositional data. Some fundamental questions and new prospects in Archaeometry and Archaeology. In Daunis-i-Estadella, J. and Martín-Fernández, J., (ed.), Proceedings of CODAWORK'08, The 3rd Compositional Data Analysis Workshop, May 27-30, 1–18. University of Girona, Girona.

299 Buxeda i Garrigós, J., Kilikoglou, V., 2003. Total variation as a measure of variability
300 in chemical data sets. In: van Zelst, L., Bishop, R. L., Henderson, J. (Ed.), Patterns and
301 Process, Smithsonian Center for Materials Research and Education, Washington DC,
302 185-198.
303
304 Carmona, P., Ruiz, J. M., 2004. Geomorphological and geoarchaeological evolution of
305 the coastline of the Tyre tombolo. Preliminary results. In: Aubet, M. E. (Ed.), The
306 Phoenician Cemetery of Tyre-Al Bass. Excavations 1997-1999, Bulletin d'Archéologie
307 et d'Architecture Libanaises I, Beirut, 207-219.
308
309 Echallier, J.-C., 1984. Éléments de technologie céramique et d'analyse des terres cuites
310 archéologiques, Documents d'Archéologie Méridionale, Numéro spécial.
311
312 Heimann, R., 1989. Assessing the Technology of Ancient Pottery: The Use of Ceramic
313 Phase Diagrams, Archaeomaterials, 3, 123-148.
314
315 Maniatis, Y., Simopoulos, A., and Kostikas, A., 1981. Moessbauer Study of the Effect
316 of Calcium Content on Iron Oxide Transformations in Fired Clays, Journal of the
317 American Ceramic Society, 64, 263-269.
318
319 Maniatis, Y., Simopoulos, A., Kostikas, A., and Perdikatsis, V., 1983. Effect of
320 Reducing Atmospheres on Minerals and Iron Oxide Devoloped in Fired Clays: the Role
321 of Ca, Journal of the American Ceramic Society, 66, 773-781.
322

MathSoft, 1999. S-PLUS. User's Guide, Data Analysis Products Division, MathSoft, Seatle.

Meier, P. C., Zund, R. E., 1993. Statistical Methods in Analytical Chemistry, Jon Wiley and Sons, New York, Santa Bárbara, Sidney and Toronto.

Núñez, F. J., 2004. Preliminary report on ceramics from the Phoenician necropolis of Tyre – al Bass. 1997 campaign. In: Aubet, M. E. (Ed.), The Phoenician Cemetery of Tyre-Al Bass. Excavations 1997-1999, Bulletin d'Archéologie et d'Architecture Libanaises I, Beirut, 281-373.

Picon, M., 1973. Introduction à l'étude technique des céramiques sigillées de Lezoux, Centre de Récherches sur les Téchniques Greco Romaines, Université de Dijon, Dijon.

Tite, M. S., Maniatis, Y., Meeks, N. Bimson, M., Hughes, M. and Leppard, S., 1982. Technological Studies of Ancient Ceramics from the Near East, Aegean and Sotheast Europe. In Wertime, T. and Wertime, S., editors, The evolution of the first fire-using industries, Smithsonian Institution Press, Washington, 61-71.

Tschegg, C., Ntaflos, T., Hein, I., 2009. Thermally triggered two-stage reaction of carbonates and clay during ceramic firing – A case study on Bronze Age Cypriot ceramics, Applied Clay Science, 43, 69-78.

Whitney, D.L., Evans, B.W., 2010. Abbreviations for names of rock-forming minerals, American Mineralogist, 95, 185-187.

Whiston, C., 1987. X-Ray Methods, Analytical Chemistry by Open Learning, Thames Polythenic, John Wiley and Sons, London.

	Coarse ware	Red slip ware	Concentric circles	Total
Jugs	25	23	1	**49**
Plates	40	11	-	**51**
Urns	1	-	-	**1**
Total	**66**	**34**	**1**	**101**

Table 1

	AB (n = 89)		**AB 1** (n = 34)		**AB 2** (n = 26)		**AB 3** (n = 11)	
	m	sd	m	sd	m	sd	m	sd
Fe_2O_3 %	6.77	0.75	6.79	0.42	7.38	0.44	5.93	0.3
Al_2O_3 %	15.48	1.68	15.21	0.77	17.27	0.94	14.85	1.3
MnO %	0.06	0.03	0.08	0.03	0.06	0.03	0.04	0.01
P_2O_5 %	0.59	0.12	0.55	0.11	0.69	0.12	0.51	0.05
TiO_2 %	0.8	0.09	0.78	0.04	0.88	0.05	0.78	0.06
MgO %	2.02	0.28	2.07	0.17	1.88	0.2	2.07	0.31
CaO %	28.61	4.54	29.38	2.36	24.65	2.87	28.49	3.11
Na_2O %	0.13	0.1	0.1	0.08	0.13	0.07	0.27	0.15
K_2O %	1.98	0.29	1.91	0.19	2.12	0.31	2.24	0.17
SiO_2 %	43.08	2.64	42.68	1.92	44.41	1.83	44.32	1.82
Ba (ppm)	3159	3540	2960	1943	3823	5736	3325	1387
Rb (ppm)	78	12	77	8	87	10	80	9
Th (ppm)	11	2	11	1	13	1	12	1
Nb (ppm)	17	2	17	2	17	3	17	2
Pb (ppm)	26	58	20	5	22	3	18	3
Zr (ppm)	155	13	155	15	159	12	159	11
Y (ppm)	35	2	34	2	35	3	35	2
Sr (ppm)	666	148	696	124	519	72	735	83
Ce (ppm)	77	11	75	10	80	10	79	10
Ga (ppm)	18	2	18	1	19	2	18	2
V (ppm)	129	16	131	10	139	16	115	11
Zn (ppm)	122	12	121	9	130	9	117	15
Cu (ppm)	47	12	50	12	47	9	31	2
Ni (ppm)	110	32	126	19	120	32	60	4
Cr (ppm)	124	14	124	10	130	16	120	17

Table 2

	TAB011	TAB012	TAB016	TAB017	TAB024	TAB031	TAB038	TAB039	TAB051	TAB067	TAB079	TAB093
Fe_2O_3 %	4.99	10.18	10.00	6.33	6.98	8.72	8.79	6.56	6.65	6.18	5.62	7.64
Al_2O_3 %	7.93	10.91	13.47	8.59	18.53	11.93	13.92	14.52	15.43	10.02	9.56	17.43
MnO %	0.11	0.18	0.16	0.13	0.05	0.18	0.16	0.07	0.04	0.09	0.09	0.05
P_2O_5 %	0.46	0.24	0.39	0.26	0.77	0.32	0.33	0.66	1.01	0.68	0.34	0.66
TiO_2 %	0.53	1.18	0.71	0.87	1.00	0.76	0.87	0.81	0.79	0.91	0.60	0.93
MgO %	1.29	5.94	3.29	11.63	2.06	4.23	5.38	2.00	2.54	1.67	1.49	4.43
CaO %	32.69	23.63	27.33	42.91	18.93	26.22	18.84	33.03	26.61	33.58	29.21	19.67
Na_2O %	0.15	0.74	1.26	0.06	0.13	0.50	1.16	0.04	0.30	0.25	0.01	0.11
K_2O %	0.48	1.21	1.31	1.35	1.96	1.35	1.69	1.61	1.56	0.71	0.70	1.72
SiO_2 %	51.14	44.79	41.79	27.71	48.83	45.47	48.36	39.90	44.55	45.54	52.15	47.04
Ba (ppm)	1058	1954	1619	7028	5853	1211	3761	6013	3750	1655	959	1598
Rb (ppm)	17	35	31	34	61	41	52	46	37	31	30	45
Th (ppm)	2	5	2	2	14	4	9	6	9	6	5	13
Nb (ppm)	13	13	9	13	15	9	12	11	13	19	15	20
Pb (ppm)	10	11	11	10	21	12	14	22	17	10	11	57
Zr (ppm)	145	121	95	154	156	119	147	158	151	271	150	174
Y (ppm)	34	25	25	14	38	25	31	28	35	38	25	39
Sr (ppm)	447	764	523	308	711	753	546	519	762	1100	532	531
Ce (ppm)	43	17	16	32	80	39	57	29	82	77	47	100
Ga (ppm)	10	13	12	10	18	12	14	15	17	11	11	20
V (ppm)	85	280	151	93	140	135	104	171	100	132	90	11
Zn (ppm)	69	99	106	45	126	89	91	100	120	110	80	145
Cu (ppm)	38	55	114	53	25	71	32	48	36	48	42	49
Ni (ppm)	74	1504	99	77	72	142	95	300	66	81	83	99
Cr (ppm)	121	6359	125	85	160	348	104	515	119	157	118	151

Table 3

Table captions

Table 1. Individuals characterized in the study

Table 2. Means (m) and standard deviation (sd) of the chemical composition groups cited in the text.

Table 3. Normalized concentrations of the 12 outliers.

Figure captions

Figure 1. Evenness chemical variability graph for all 101 individuals characterized. vt: total variation. $\tau_{,i}$: trace of the covariance matrix in ALR transformation using that element as divisor

Figure 2. Dendrogram of all 101 individuals after a cluster analysis performed on the subcomposition Fe_2O_3, Al_2O_3, MgO, CaO, K_2O, SiO_2, Rb, Th, Nb, Zr, Y, Sr, Ce, Ga, V, Zn, Ni and Cr, ALR transformed using TiO_2 as divisor

Figure 3. Dendrogram on the 89 individuals of group AB after a cluster analysis performed on the subcomposition Fe_2O_3, Al_2O_3, MgO, CaO, K_2O, SiO_2, Rb, Th, Nb, Zr, Y, Sr, Ce, Ga, V, Zn, Ni and Cr, ALR transformed using TiO_2 as divisor

Figure 4. Histogram of Ba concentrations in normalized data for all 101 individuals

Figure 5. Ceramic diagram with the individuals in subgroups AB 1, AB 2 and AB 3. An = anorthite ($CaAl_2Si_2O_8$); Mul = mullite ($3Al_2O_3 \cdot 2SiO_2$); Gh = gehlenite ($Ca_2Al_2SiO_7$); Wo = wollastonite ($CaSiO_3$); Qz = quartz (SiO_2). Abbreviations after Whitney and Evans 2010

Figure 6. XRD spectra. Upper left: TAB022, as representative of individuals in AB group. Upper right: TAB042, individual in group AB with the higher concentration in baryte. Lower left: outlier TAB012 of possible Cypriot origin. Lower right: outlier TAB017 rich in dolomite. Ba: baryte. Cal: calcite. Di: pyroxene. Dol: dolomite. Gh: gehlenite. Hem: hematite. Ilt: illite-muscovite. Kfs: potassium feldspars. Mrbk: amphibole. Pl: plagioclase. Qz: quartz. Abbreviations after Whitney and Evans 2010

Figure 7. SEM microphotrographs. TAB003: representative of AB individuals exhibiting a non vitrification stage matrix. TAB070: secondary baryte in pores. TAB017: possible crystals of dolomite temper. TAB012: initial vitrification / continous vitrification (Vc-) stage matrix

Figure1

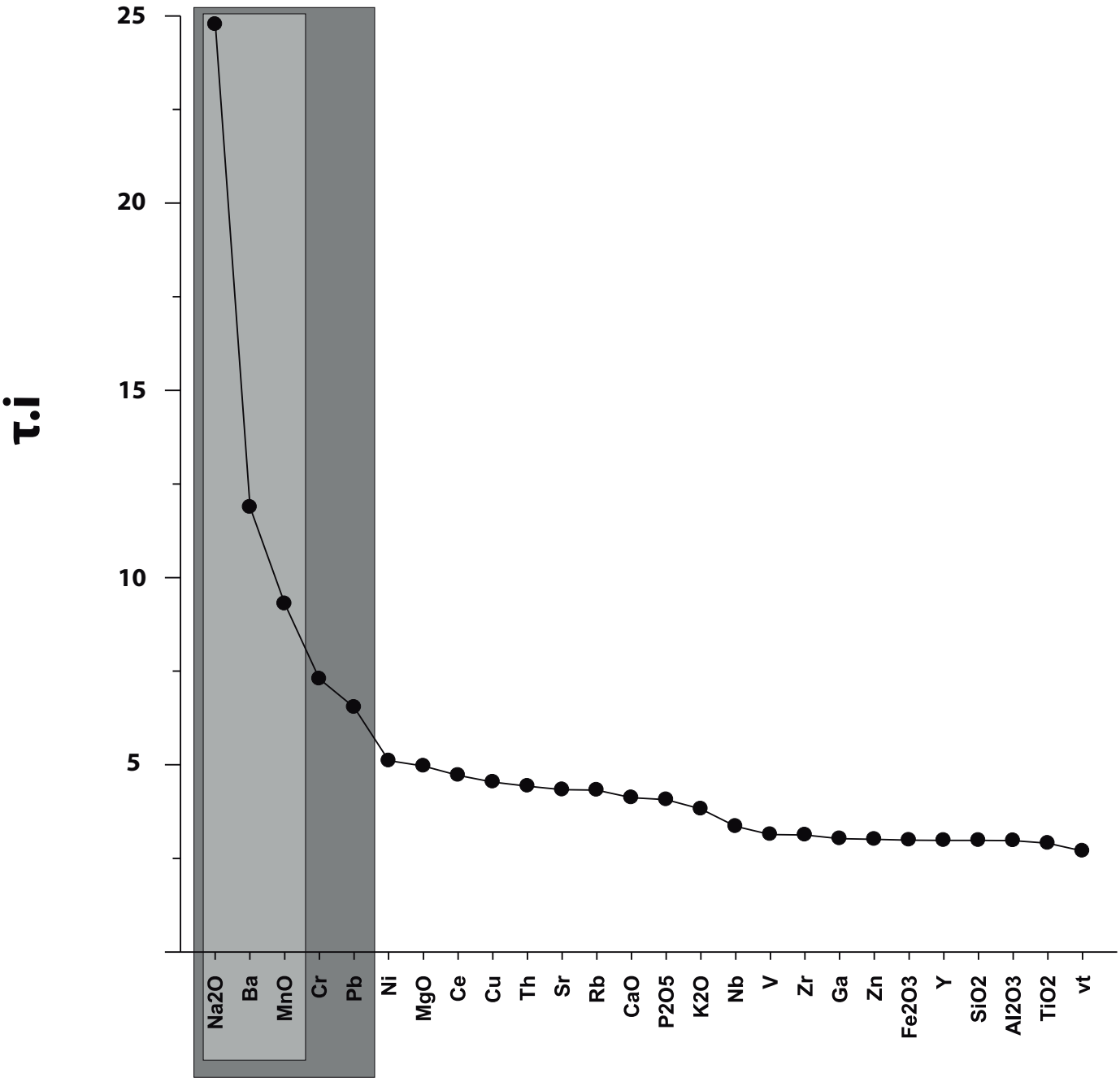
τ.i
25
20
15
10
5
Na2O
Ba
MnO
Cr
Pb
Ni
MgO
Ce
Cu
Th
Sr
Rb
CaO
P2O5
K2O
Nb
V
Zr
Ga
Zn
Fe2O3
Y
SiO2
Al2O3
TiO2
vt

Figure2

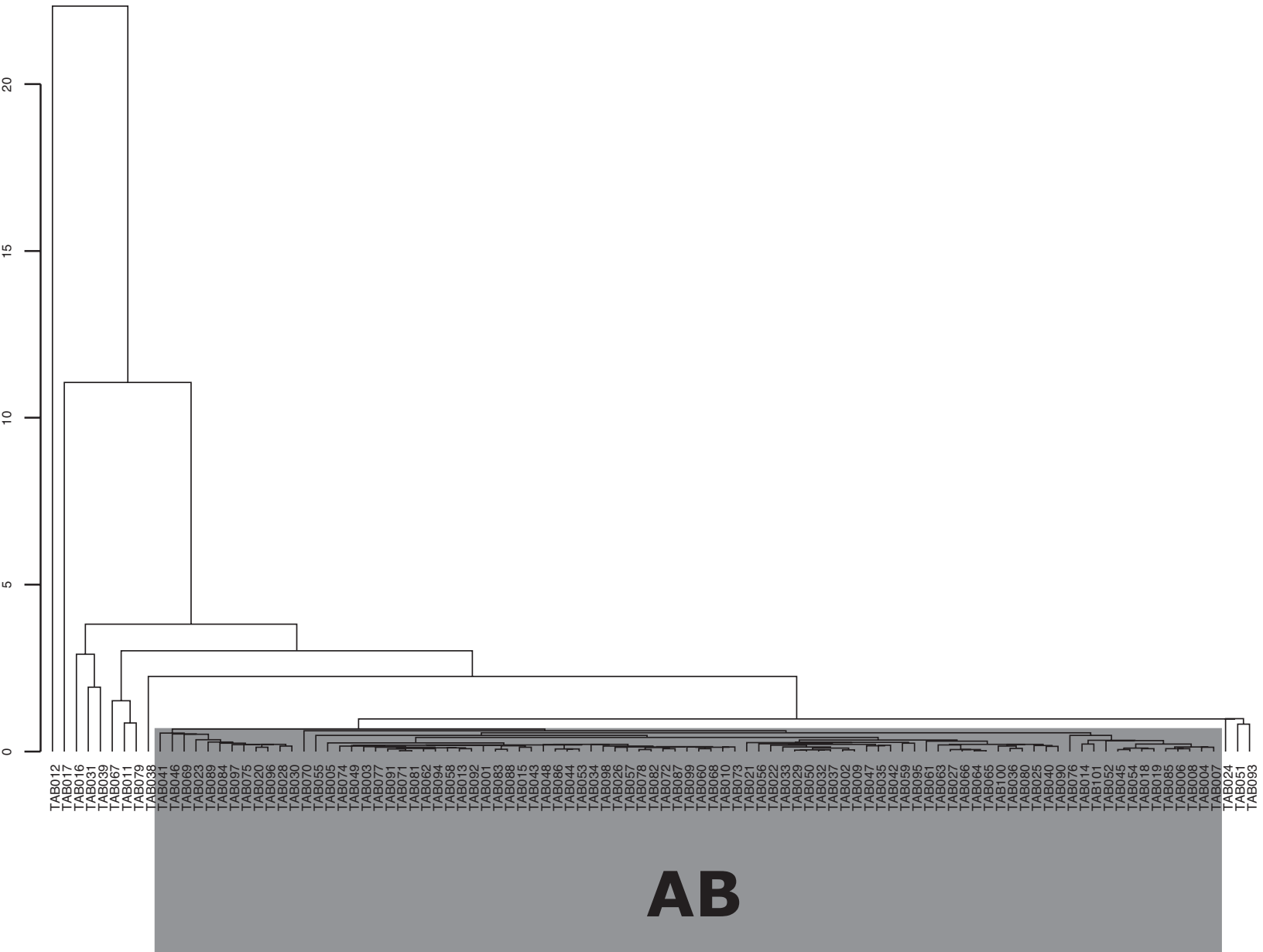
0
5
10
15
20
TAB012
TAB017
TAB016
TAB031
TAB039
TAB067
TAB011
TAB079
TAB038
TAB041
TAB046
TAB069
TAB023
TAB089
TAB084
TAB097
TAB075
TAB020
TAB096
TAB028
TAB030
TAB070
TAB055
TAB005
TAB074
TAB049
TAB003
TAB077
TAB091
TAB071
TAB081
TAB062
TAB094
TAB058
TAB013
TAB092
TAB001
TAB083
TAB088
TAB015
TAB043
TAB048
TAB086
TAB044
TAB053
TAB034
TAB098
TAB026
TAB057
TAB078
TAB082
TAB072
TAB087
TAB099
TAB060
TAB068
TAB010
TAB073
TAB021
TAB056
TAB022
TAB033
TAB029
TAB050
TAB032
TAB037
TAB002
TAB009
TAB047
TAB035
TAB042
TAB059
TAB095
TAB061
TAB063
TAB027
TAB066
TAB064
TAB065
TAB100
TAB036
TAB080
TAB025
TAB040
TAB090
TAB076
TAB014
TAB101
TAB052
TAB045
TAB054
TAB018
TAB019
TAB085
TAB006
TAB008
TAB004
TAB007
TAB024
TAB051
TAB093
AB

Figure3

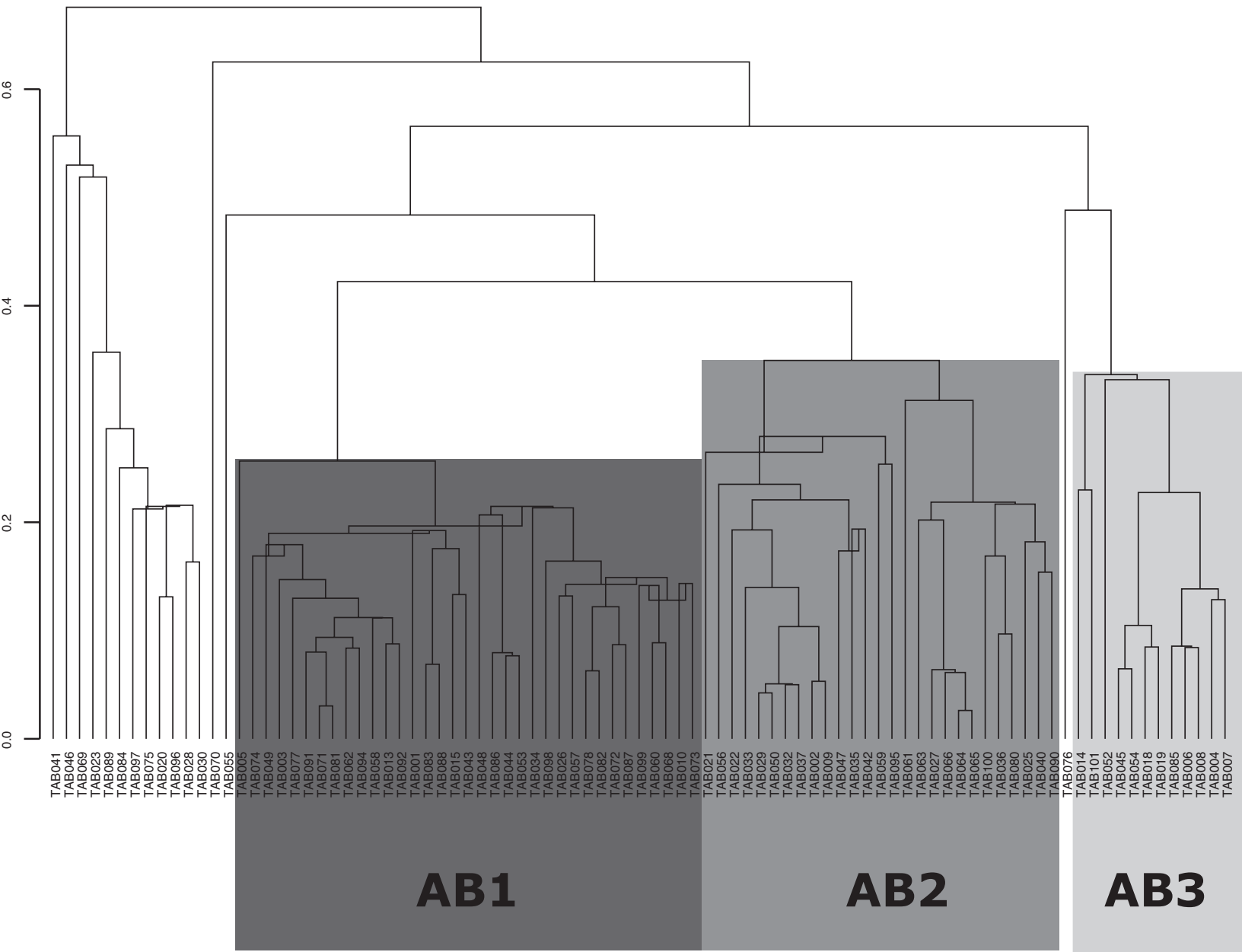
0.0
0.2
0.4
0.6
TAB041
TAB046
TAB069
TAB023
TAB089
TAB084
TAB097
TAB075
TAB020
TAB096
TAB028
TAB030
TAB070
TAB055
TAB005
TAB074
TAB049
TAB003
TAB077
TAB091
TAB071
TAB081
TAB062
TAB094
TAB058
TAB013
TAB092
TAB001
TAB083
TAB088
TAB015
TAB043
TAB048
TAB086
TAB044
TAB053
TAB034
TAB098
TAB026
TAB057
TAB078
TAB082
TAB072
TAB087
TAB099
TAB060
TAB068
TAB010
TAB073
TAB021
TAB056
TAB022
TAB033
TAB029
TAB050
TAB032
TAB037
TAB002
TAB009
TAB047
TAB035
TAB042
TAB059
TAB095
TAB061
TAB063
TAB027
TAB066
TAB064
TAB065
TAB100
TAB036
TAB080
TAB025
TAB040
TAB090
TAB076
TAB014
TAB101
TAB052
TAB045
TAB054
TAB018
TAB019
TAB085
TAB006
TAB008
TAB004
TAB007
AB1
AB2
AB3

Figure4
Click here to download high resolution image

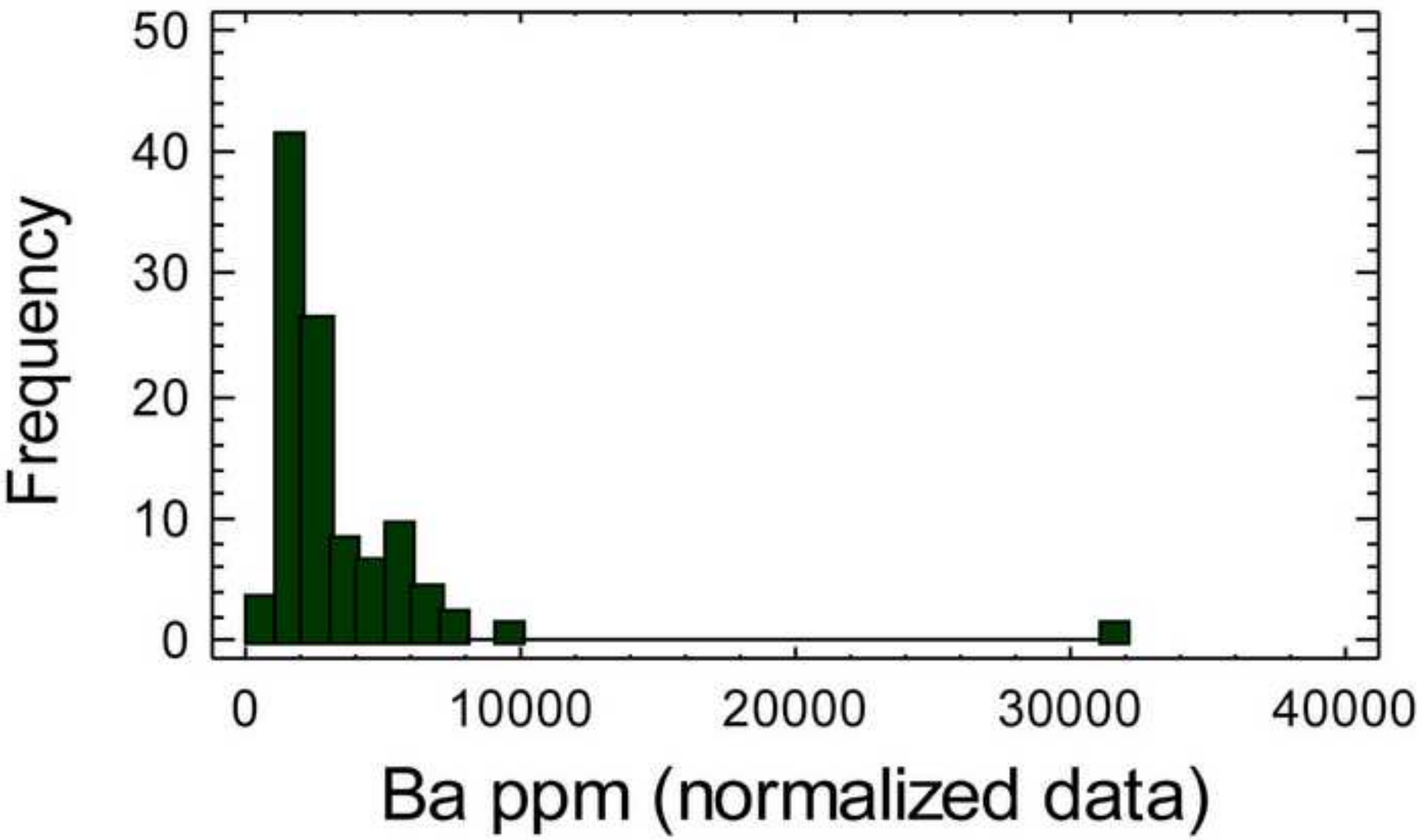

Figure5

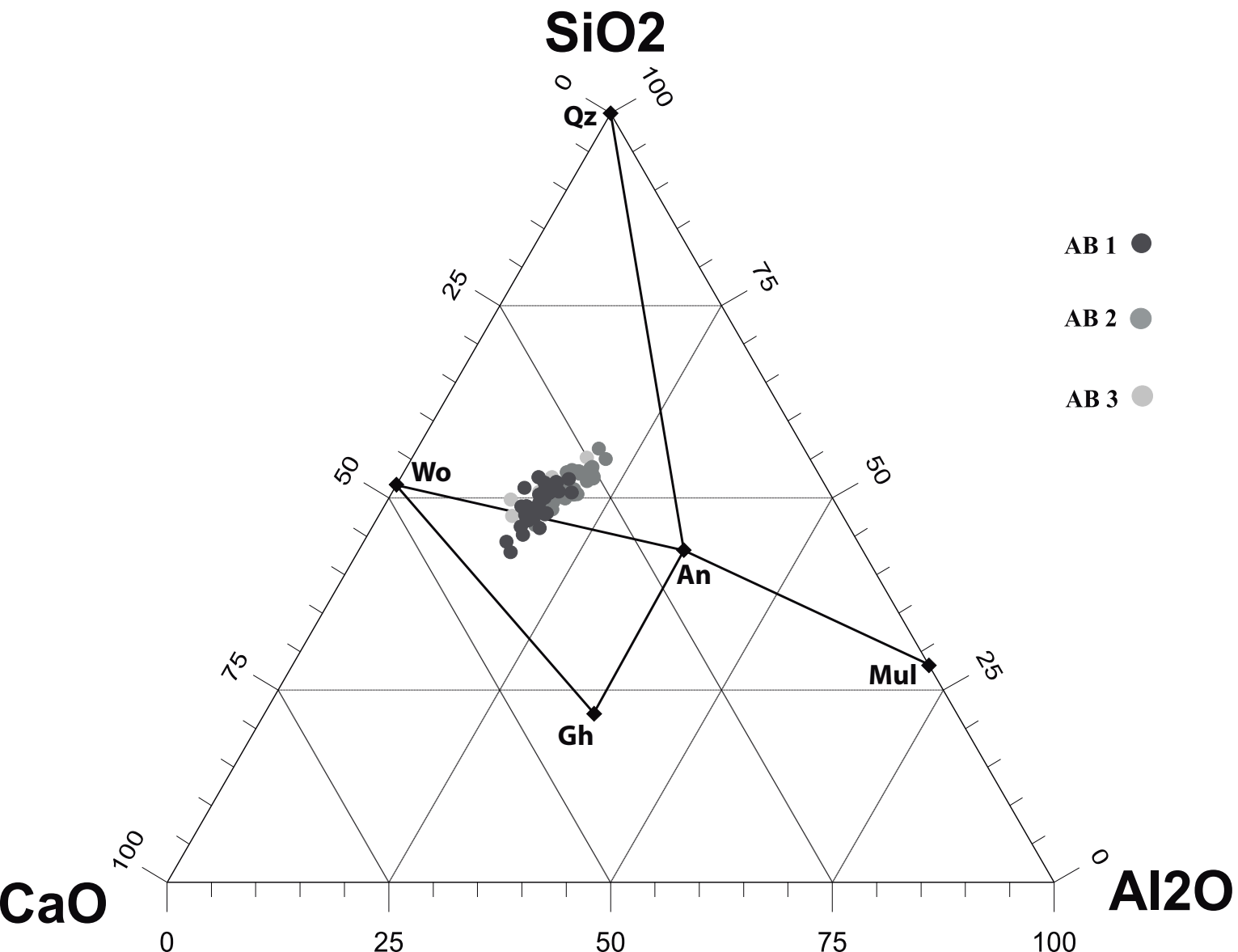
SiO2
0
100
Qz
25
75
AB 1
AB 2
AB 3
50
Wo
50
An
75
Mul
25
Gh
100
0
CaO
Al2O
0
25
50
75
100

Figure6

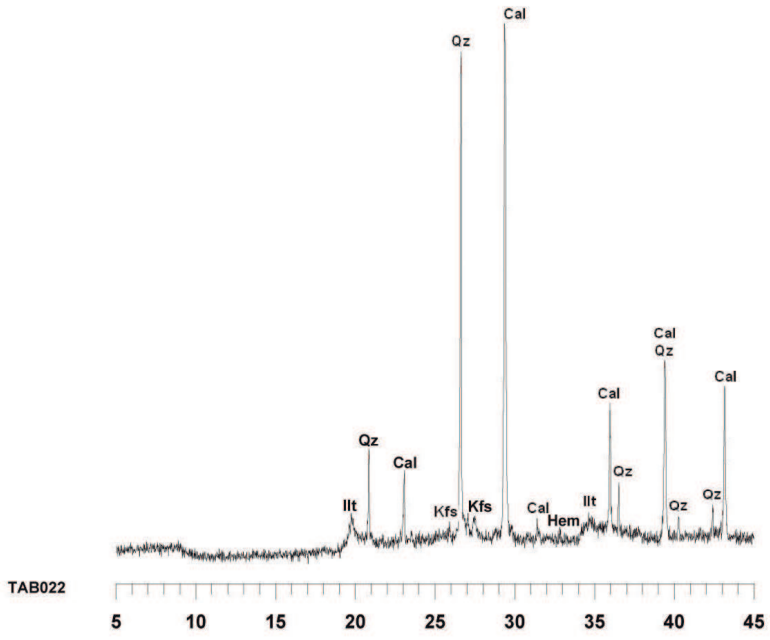
Cal
Qz
Qz
Cal
Ilt
Kfs
Kfs
Cal
Hem
Ilt
Cal
Qz
Oz
Cal
Oz
Oz
Oz
TAB022
5
10
15
20
25
30
35
40
45

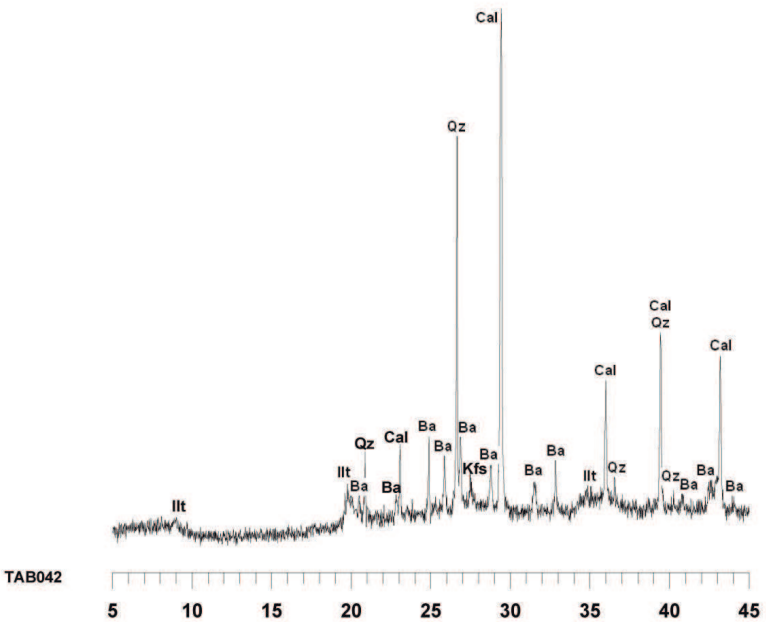
Cal
Qz
Cal
Oz
Cal
Cal
Qz
Ba
Ba
Ba
Ba
Kfs
Ba
Ba
Ba
Ba
Ilt
Ba
Ba
Ilt
Qz
Qz
Ba
Ba
Ba
Ilt
Ba
Ba
Ba
Ba
Ba
TAB042
5
10
15
20
25
30
35
40
45

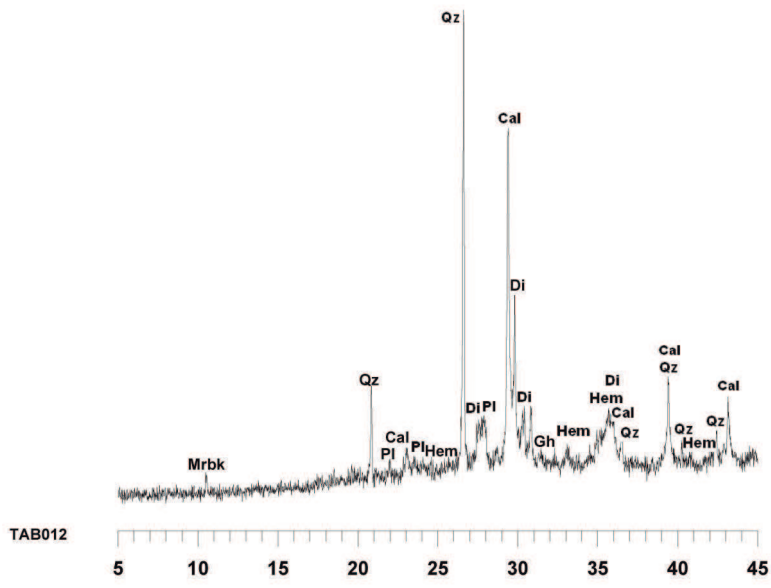
Qz
Cal
Di
Di
Pl
Di
Di
Hem
Cal
Qz
Cal
Qz
Qz
Cal
Pl
Pl
Hem
Gh
Hem
Qz
Hem
Qz
Mrbk
TAB012
5
10
15
20
25
30
35
40
45

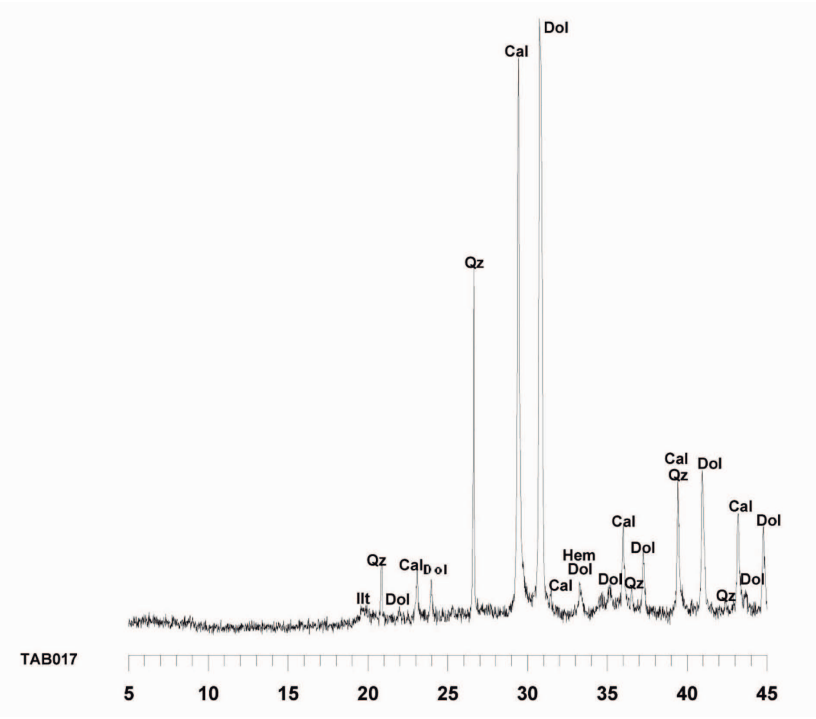
Dol
Cal
Qz
Cal
Qz
Dol
Cal
Dol
Cal
Dol
Hem
Dol
Dol
Qz
Cal
Dol
Qz
Cal
Dol
Qz
Ilt
Dol
Cal
Dol
TAB017
5
10
15
20
25
30
35
40
45

Figure7

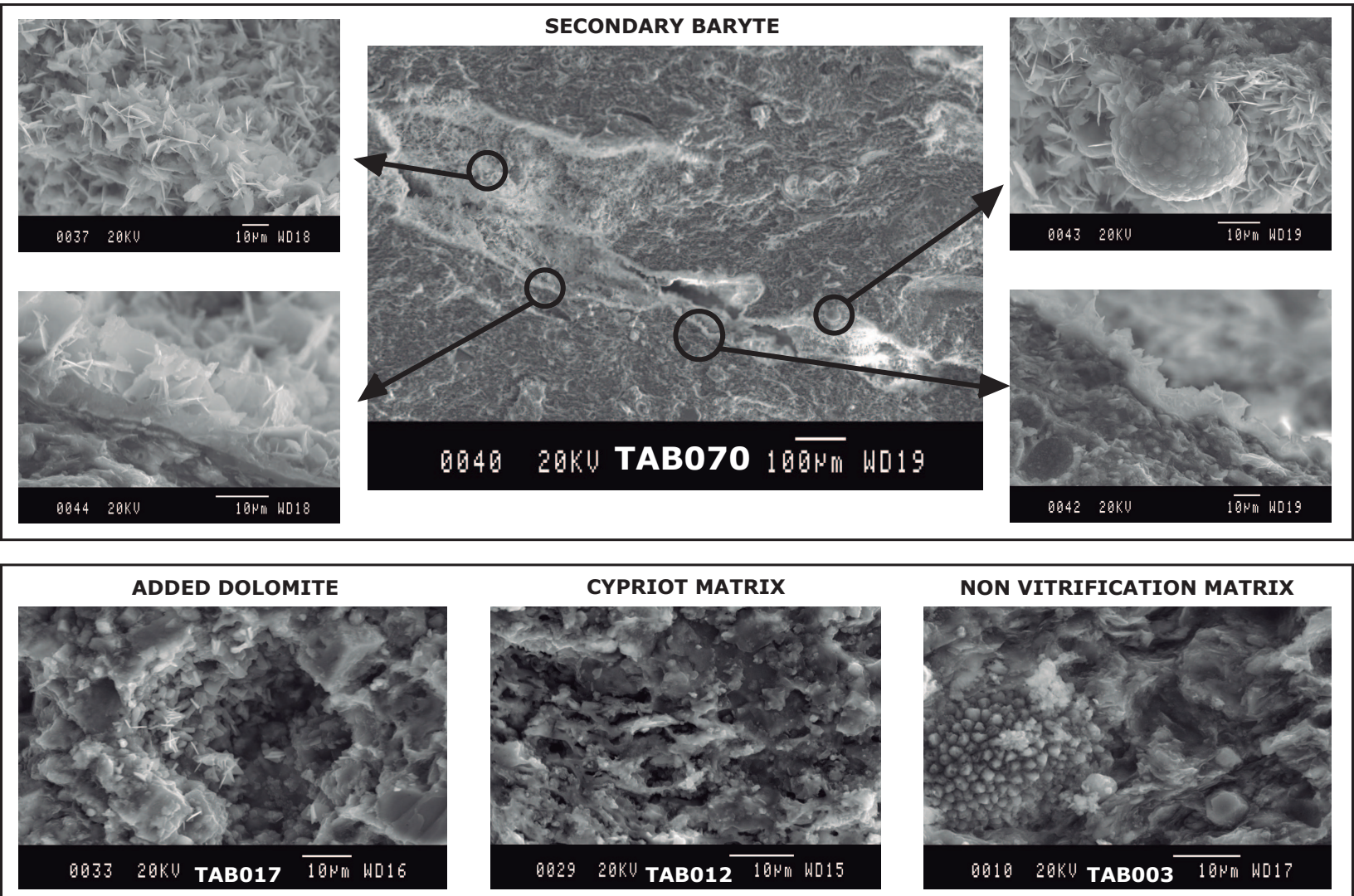
SECONDARY BARYTE
0037 20KV 10µm WD18
0044 20KV 10µm WD18
0040 20KV TAB070 100µm WD19
0043 20KV 10µm WD19
0042 20KV 10µm WD19
ADDED DOLOMITE
0033 20KV TAB017 10µm WD16
CYPRIOT MATRIX
0029 20KV TAB012 10µm WD15
NON VITRIFICATION MATRIX
0010 20KV TAB003 10µm WD17